ELSEVIER

Tectonophysics 359 (2002) 29–46

TECTONOPHYSICS

www.elsevier.com/locate/tecto

Velocity field for crustal deformation in China derived from seismic moment tensor summation of earthquakes

Changyuan Qin[1], Constantinos Papazachos*, Eleftheria Papadimitriou

Geophysical Laboratory, School of Geology, University of Thessaloniki, P.O. Box 352-1, Thessaloniki GR-54006, Greece

Received 15 November 2001; accepted 10 July 2002

Abstract

The intraplate motion is studied in the territory of China where about 150 polygonal seismic sources are considered and grouped on the basis of the available fault plane solutions, large known faults and level of seismic activity. Every polygon is divided into several triangles and velocities at the triangle vertices are determined from the available moment rate tensors by assuming a linear continuity of the velocity field within each triangle. The estimation of the moment rate tensor is partitioned in the unit-scaled moment tensor obtained by the available fault plane solutions of large event ($M \geq 5.0$) after 1900, which define the type of deformation and the scalar annual moment rate, obtained by the complete seismicity catalogue which defines the rate of seismic deformation. The results show that the convergence between India and Eurasia is about 50 mm/year with Eurasia fixed, while the eastern part of China moves eastwards at about 8–10 mm/year. The motion direction changes gradually from northeastward around the Himalayan region to southeastward around the Red River fault and to southwestward around eastern Himalayan Syntaxis, which partially compensates the penetration of the Indian plate. A sharp change of the velocity gradient was found near the southeastern part of Tibet plateau, the Qilianshan region and Fuyun fault where large strain rates are released due to strong earthquakes there. The results are supported by recent horizontal GPS motion model and other independent evidence. The motion pattern between the Altun–Qilianshan–Longmenshan faults and the Himalayan fault in Qinghai–Tibet region strongly suggests that this area exhibits a more or less continuous deformation pattern rather than a rigid block behavior.

Keywords: China; Seismicity; Moment rate; Crustal deformation

1. Introduction

Crustal deformation takes place not only at the plate boundaries, according to the hypothesis of plate tectonics, but also along broad intraplate zones (Madariaga, 1983; Peltzer, 1988). Displacement across faults is associated with great earthquakes, which represent the episodic slip at the brittle interface between plates. The total slip accumulated during large earthquakes in a given segment of a fault corresponds very closely to the rate of relative motion between the plates determined by other non-seismological methods (Madariaga, 1983). Thus, earthquakes are due to the rapid release of strain energy that has been

* Corresponding author.

E-mail addresses: qin@lemnos.geo.auth.gr (C. Qin), costas@lemnos.geo.auth.gr (C. Papazachos).

[1] Now at the School of Environmental Sciences, University of East Anglia, NR4 7TJ Norwich, UK.

0040-1951/02/$ - see front matter © 2002 Published by Elsevier Science B.V.
PII: S0040-1951(02)00401-8

concentrated in the vicinity of the fault zone by the slow deformation of the lithosphere. Peltzer and Saucier (1996) showed that long-term deformation within continents is mostly localized into major faults. Thus, the motion of quasi-rigid blocks of the earth's crust can be used to describe the corresponding velocity field (Haines, 1982). The moment tensors, which are related to the size of the corresponding earthquakes, can be used to determine the crustal deformation of a seismogenic volume (Kostrov, 1974; Jackson and McKenzie, 1988; Ward, 1998a,b).

The relationship between the seismic deformation and the moment has been discussed in detail (Jackson and McKenzie, 1988; Westaway, 1991, 1995; Savage and Simpson, 1997). Haines (1982) proposed a

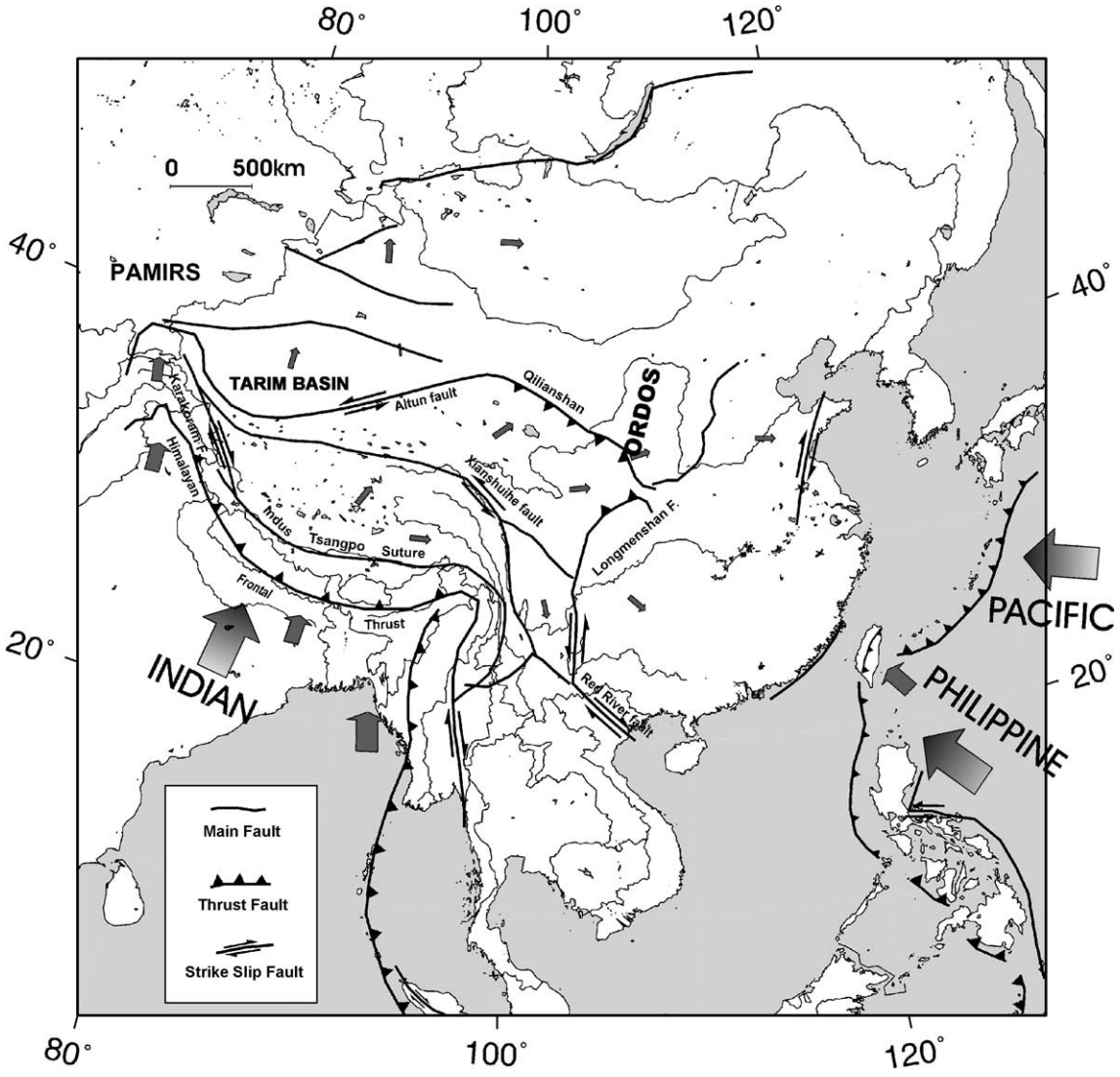

Fig. 1. The distribution of major faults zones within the broader China area. Small gray arrows indicate the local motion, as this is determined by geological/tectonic field observations (Ma, 1987). The large labeled arrows indicate the average motion of the Indian, Pacific and Philippine plates.

method that allows to uniquely obtain the general horizontal velocity field, where he showed that with a generally variable strain field in which the rates of horizontal shear strain are everywhere known, the complete horizontal velocity field can be recovered if one line remains unstrained. Therefore, the key to obtaining the horizontal velocity field occurring across and within zones of distributed deformation lies in the ability to determine the spatial variation in the strain rate field (Haines and Holt, 1993). Different methods, based on these concepts, have been used to model the motion of the earth's crust (Holt et al., 1991, 1995; Haines and Holt, 1993; Peltzer and Saucier, 1996; England and Molnar, 1997a,b).

Crustal deformation in the mainland of China is mainly due to the strong northeastward motion of the Indian plate at southwest China (all the motions are relative to "stable" Eurasia, unless otherwise specified), the westward subduction of Pacific plate beneath East China and the northwestward impact of the Philippine plate (Fig. 1) (Chen and Molnar, 1977; Deng et al., 1994). Kinematic and dynamic processes are mainly controlled by these plate motions (Ma, 1987; Xu and Deng, 1996; Qin et al., 1999a), which are related to the formation of large faults and high seismic activity. Because of the complexity of the joint motions, different types of regional faults are found that are more or less responsible for the local motion.

In the framework of the present work, about 150 polygonal seismic sources of 10 seismotectonic zones are determined in the mainland of China and its surrounding area based on the geological and seismotectonic characteristics, the known fault plane solutions and the seismic activity. Based on the moment rate calculated from the maximum magnitude and the parameters from magnitude–frequency relation, as well as the moment tensor decomposition method (Papazachos and Kiratzi, 1992), the velocity field with respect to Eurasia is quantitatively determined by the complete earthquake data set (Qin et al., 1999a) and the regional focal mechanisms. The model stain rate field is compared with the one directly obtained from moment rate for the validation of the method. Moreover, the velocity field with Eurasia fixed is compared with the GPS' one using the kinematic model given by Zhang and Zhou (1998), which was obtained from GPS measurements collected between 1994 and 1996.

2. Data and seismotectonic setting

In order to estimate the seismic deformation in the study area, it is necessary to have a reliable seismicity catalogue, as well as an adequate number of fault plane solutions (see "Electronic Supplements" on the journal's homepage http://www.elsevier.com/locate/tecto). The catalogue used for the purpose of the present study is distributed by the China Seismological Bureau (CSB) of P.R. China and covers the time period from 1800 A.D. to 1995, containing earthquakes with equivalent moment–magnitudes $M \geq 5.0$. This catalogue was checked in comparison with the catalogues of Pacheco and Sykes (1992) and Abe (1981), as well as with the ISC bulletins since 1966 and modified accordingly. The completeness of the data used in the present study (Table 1) is the one proposed by Qin et al. (1999a), which has been defined studying the low-magnitude linearity cut-off of the Gutenberg–Richter relation for data of different time periods, as well as time behavior of the cumulative number of the events (Qin et al., 1999a). The catalogue was updated until the beginning of 2000 and extended in order to include northern India, Mongolia and the southern part of Siberia (Fig. 2).

For the fault plane solutions only those with magnitude $M \geq 5.0$ were used, in order to have a relative reliable data set, resulting in 735 fault plane solutions of earthquakes which have occurred since 1900. Most of the data were determined using first motions from long period recordings or from waveform modeling. A small part of the fault plane solutions were derived from field observations and aftershock sequences. In many case when more than one fault plane solutions were available for the same event, especially the large ones, the waveform modeling solution (e.g. Harvard CMT, etc.) was preferred. Four main zones of similar faulting pattern can be outlined by the fault plane solutions for the broader China area (Fig. 3).

Table 1
Completeness information for the seismicity data used in the present study

Magnitude	Time interval
$M \geq 8.0$	1800–2000
$8.0 > M \geq 6.0$	1900–2000
$6.0 > M \geq 5.0$	1950–2000

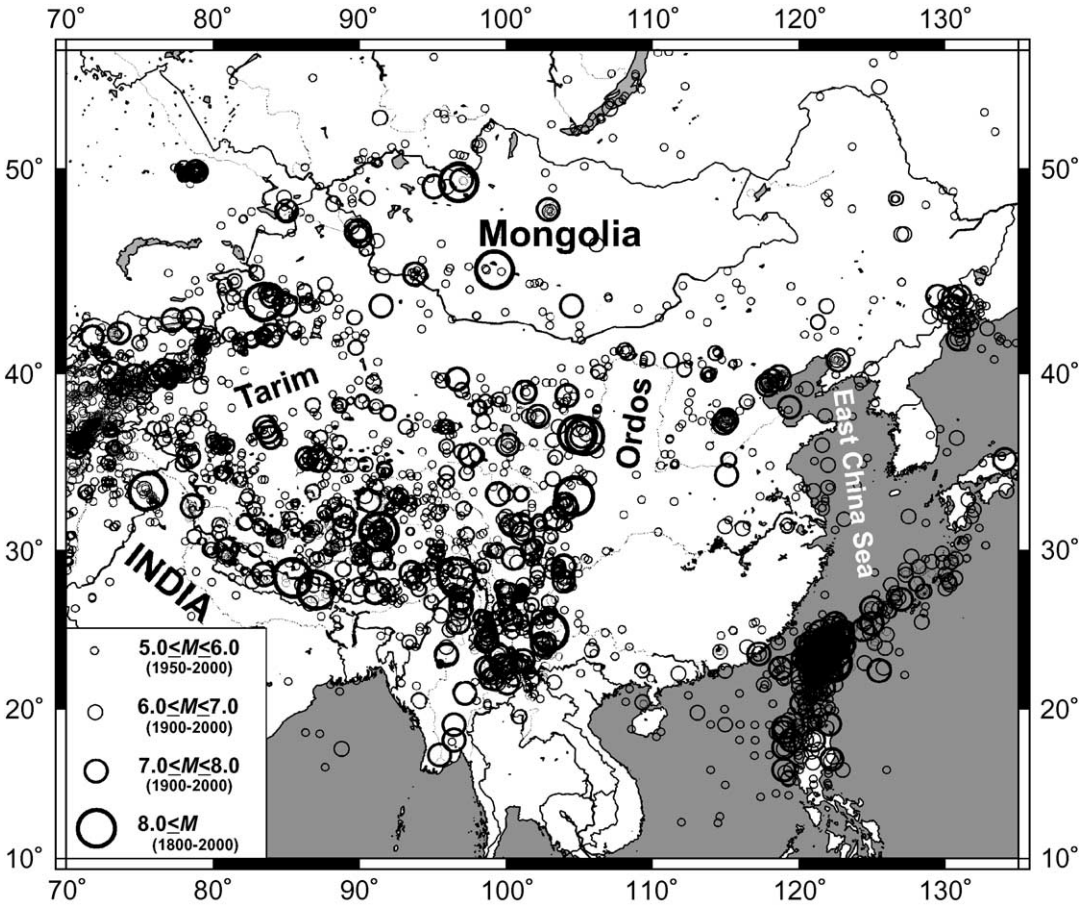

Fig. 2. Distribution of the epicenters of the complete catalogue used in the present study.

2.1. Thrust faulting zone around the Himalayans

The Himalayan front in southwest China is characterized by compression and is undergoing rapid uplift (Molnar and Lyon-Caen, 1989; Gao, 1996) due to the intrusion of Indian plate, with fault planes dipping northwards. Bouguer anomalies are increasingly dominated by negative values as we move northwards from India towards China, indicating that the crust is thickening in this direction (Kearey and Vine, 1990). The overall pattern of fault plane solutions is compatible with the subduction of the Indian plate in front of the Himalayan Frontal Thrust. The continuous uplift of this zone accommodates part of the material accretion by the intrusion (Molnar and Lyon-Caen, 1989).

2.2. Thrust faulting zone in the northwestern part of China and its surrounding areas

The northwest part of China is also supposed to be controlled by thrust faulting. It extends from the eastern boundary of Tarim basin, passing the Tien Shan thrust fault, to the area out of China (Kazakhstan, etc.) (Avouac et al., 1993). This zone is believed to be the place that absorbs most of the ''rheological-type'' of deformation caused by the penetration of the Indian plate. England and Molnar (1997a) have suggested that the continental lithosphere of Asia is more properly regarded as belonging to the ''fluid'' portion of the solid earth than to the relatively small fraction of Earth that behaves as a rigid plate.

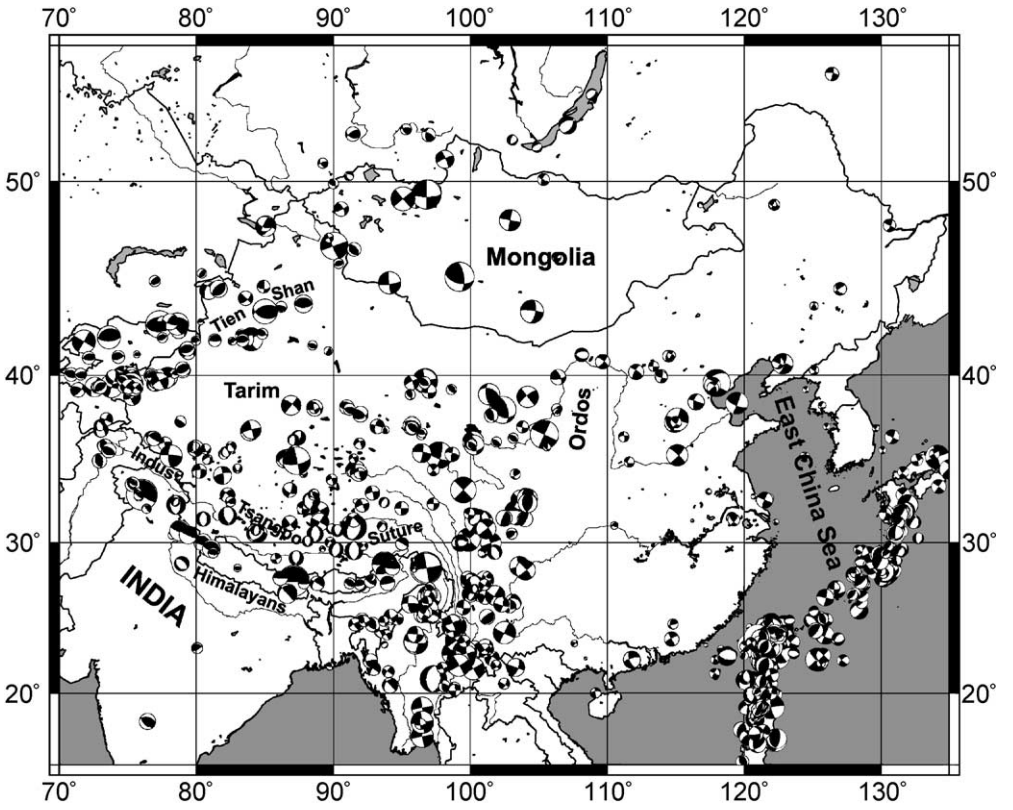

Fig. 3. The fault plane solutions distribution around the territory of China and its nearby regions.

2.3. Normal faulting zone along the Indus Tsangpo Suture

A large normal faulting zone runs along the Indus Tsangpo Suture. Almost all the *T*-axes of the fault plane solutions have an east–west direction (Qin et al., 2001). These normal faults are located at higher altitude (>5000 m) and gradually change to strike–slip faults with the decrease of altitude northwards (Molnar and Lyon-Caen, 1989). Several possible explanations have been presented about these normal faults. England and Houseman (1988) explained the formation of these normal faults as a result of thermal activity.

2.4. Strike–slip faulting zone

Strike–slip motion is the main type of deformation in the territory of China. Houseman and England (1993), by employing rheological models, pointed out that a large part of the indentation of the Indian plate has been accommodated by eastward motion of the lithosphere blocks of southeastern China. They claimed that the total north–south shortening strain caused by the Indian impact is partitioned between crustal thickening and eastward displacement in the ratio of 3:1 and 4:1. Molnar and Lyon-Caen (1989) argued that about one-third of the indentation is excluded eastwards out of the Tibet block. Recent views favor a rheological model for the Asia rather than the traditional rigid block approach (Molnar and Gipson, 1996; England and Molnar, 1997a; Wen and Anderson, 1997).

3. Method

The estimation of the velocity field was performed in a two-step process. The first step concerns the estimation of the strain-rate tensor following the

method of Kostrov (1974), as this is modified by Papazachos and Kiratzi (1992). In the second step, the velocity field is quantitatively estimated from the strain rate by means of a finite element method (England and Molnar, 1997b). These two steps of the applied method are described in detail in the following.

3.1. Estimation of strain rate tensor

The average strain rate of a seismogenic volume for a non-simple shear region can be obtained through the moment tensor summation technique (Kostrov, 1974):

$$\dot{\varepsilon}_{ij} = \frac{1}{2\mu V\tau}\sum_{n=1}^{N} M_{ij}^{n} = \frac{1}{2\mu V\tau} M_{ij} \qquad (1)$$

where μ is the shear modulus (for the present study $\mu = 3.3\mathrm{e}-11$ dyn/cm^2; Research Group of SSB, 1988); τ the time interval spanned by the data; N the number of earthquakes in the volume V (thickness of the seismogenic volume is assumed to be 15 km), M_{ij}^{n} the nth earthquake's moment tensor element, and M_{ij} the sum of moment tensor in the seismogenic volume V. The moment tensors can be easily estimated from the focal mechanisms using the relations of Aki and Richards (1980). It should be noted that the coordinate system used was the East(x)–North(y)–Up(z) system, which has been adopted throughout the present study.

For a simple shear region Westaway (1991) modified the above formulae by giving a modified tensor that reveals valid information about the deforming region. Since the largest part of China is mostly dominated by the strike slip with thrust/normal components, we do not expect to have a pure simple shear region, hence the application of relation (1) can be considered as valid for the present paper.

To avoid problems in the application of relation (1) in the cases when seismic faults intersect the boundary of each studied seismogenic zone (Molnar, 1983), we have separated the examined area in 10 seismogenic zones (Fig. 4), which have been defined by Qin et al. (2001). These zones follow the trend of major faults and are relatively large in comparison with the fault dimensions. On the other hand, it has been pointed out that there is more information in the individual moment tensors (i.e. motion) of earthquakes in a deforming seismogenic volume than is described by the sum of the moment tensors across the zone (Jackson and McKenzie, 1988). It is therefore necessary to split each deforming zone into smaller regions of relatively homogeneous deformation, before estimating the summed moment tensors. Therefore, more than 150 polygonal seismic sources were defined on the basis of geological and seismotectonic characteristics as well as the seismic activity and available focal mechanisms (Qin et al., 1999b, 2001), also shown in Fig. 4. Each source has been further divided into triangles for the application of the finite-element method, later described.

For the application of Eq. (1) it is necessary that the moment tensor data be complete during the time interval τ, otherwise the calculated strain rate will be underestimated. However, this condition is rarely met, especially for historical events. In general, the seismicity data are complete over much larger time periods than the fault plane solutions. To overcome this problem, we have applied the decomposition method proposed by Papazachos and Kiratzi (1992) according to which the annual moment rate tensor can be partitioned in two independent quantities, namely the unit-scaled moment tensor $\overline{\overline{m}}$ and the scalar seismic moment rate $\dot{M}_o$. The unit-scaled moment tensor $\overline{\overline{m}}$, which describes the "shape" of the deformation can be estimated from all the reliable focal mechanism data and/or geological data. On the other hand, the scalar seismic moment rate, $\dot{M}_0$, can be estimated from the complete seismicity data, which are usually available for much larger time periods. Following this approach, relation (1) can be written as:

$$\dot{\varepsilon} = \frac{1}{2\mu V\tau} M_0\overline{\overline{m}} = \frac{1}{2\mu V}\dot{M}_0\overline{\overline{m}} \qquad (2)$$

The unit-scaled or "shape" tensor $\overline{\overline{m}}$ can be estimated from all the focal mechanisms available for the studied region, regardless of their completeness, using equation:

$$\overline{\overline{m}}_{ij} = \frac{\sum_n M_{ij}^{n}}{\sum_n M_0^{n}} \qquad (3)$$

where M_{ij}^{n} is the ijth component of the moment tensor of the nth focal mechanism and M_0^{n} is its corresponding

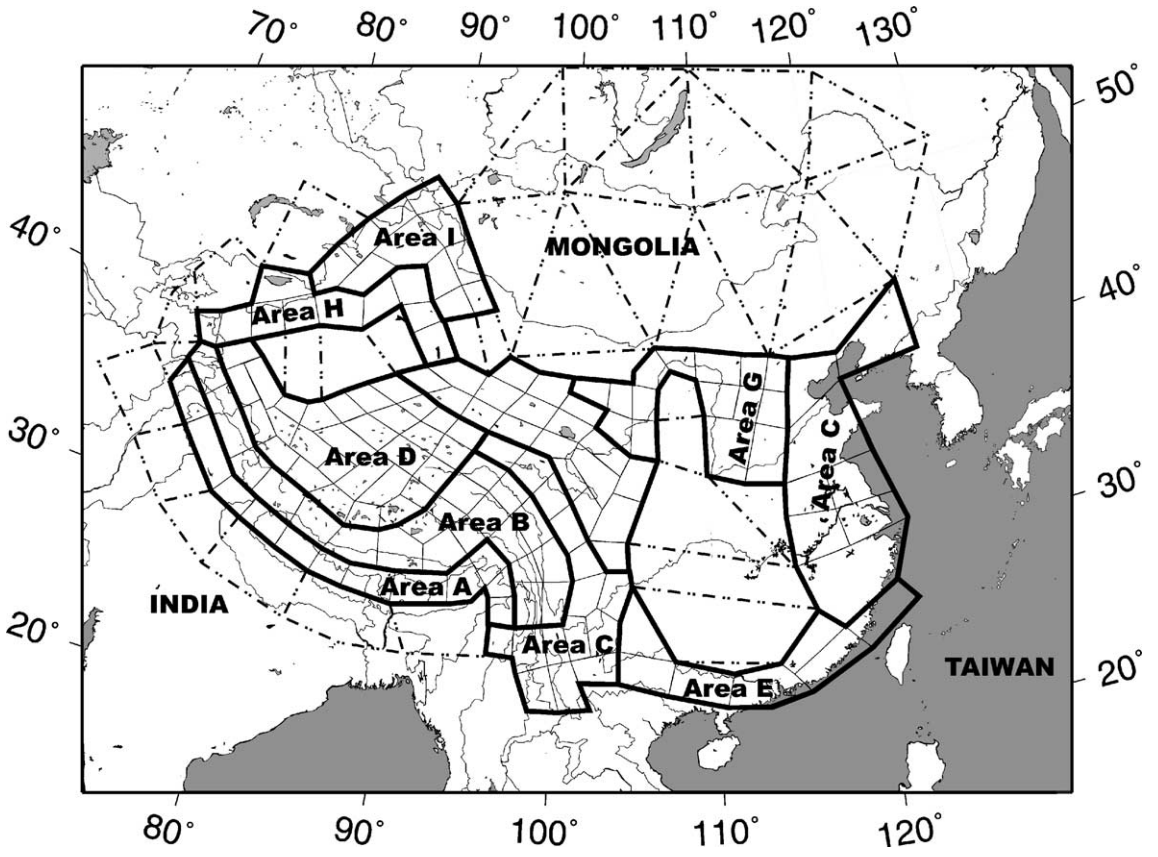

Fig. 4. Division of the study area into 10 main seismotectonic zones (thick solid lines) and 147 polygons (dashed lines) inside the mainland of China, on the basis of seismotectonic information, fault plane solutions and seismicity level of the broader China mainland. The less active dot-dashed zones outside the China mainland have been defined only by seismicity level and the available fault plane solutions.

scalar moment. When more than one fault plane solutions are available in a region the bigger earthquakes have larger weight (larger M_0) than that of the small ones for the calculation of the representative "shape" tensor, $\overline{\overline{m}}$, as can be seen from Eq. (3). This reflects their larger significance for regional tectonics but is also convenient as larger earthquakes usually have more reliable fault plane solutions than the smaller ones.

For the scalar seismic moment rate $\dot{M}_0$, it was calculated from the complete seismic data set following the formulation suggested by Molnar (1979), which employs the following equation:

$$\dot{M}_0 = \frac{\alpha}{1-\beta} M_{0,\max}^{1-\beta}$$
$$\alpha = 10^{\left(a-\frac{bd}{c}\right)},\ \beta = \frac{-b}{c} \qquad (4)$$

where a and b are the parameters of the Gutenberg–Richter relation, c and d are the coefficients of the empirical moment–magnitude relation taken equal to 1.5 and 16.1, respectively, in the present study (Kanamori, 1977; Ekstrom and Dziewonski, 1988) and $M_{0,\max}$ is the moment released by the maximum earthquake in the examined area. Since Eq. (4) is based on an integration of the released moment through the Gutenberg–Richter relation, the contribution of smaller magnitude events ($M < 5.0$) is indirectly taken into account in the estimation of the total deformation. The contribution of such events can be quite significant and is often equal to the contribution of large magnitude events (e.g. Ambraseys and Jackson, 1997). However, since the relation between the slip-sense of small- and large-magnitude events is still not well understood, the application of Eq. (4) should

be limited to small areas (sources) of more or less homogeneous seismicity and faulting pattern, such as the ones defined in the present study.

Since the seismicity catalogue had different completeness for various time periods (see Table 1), we have used the ‘‘mean value method’’ (Milne and

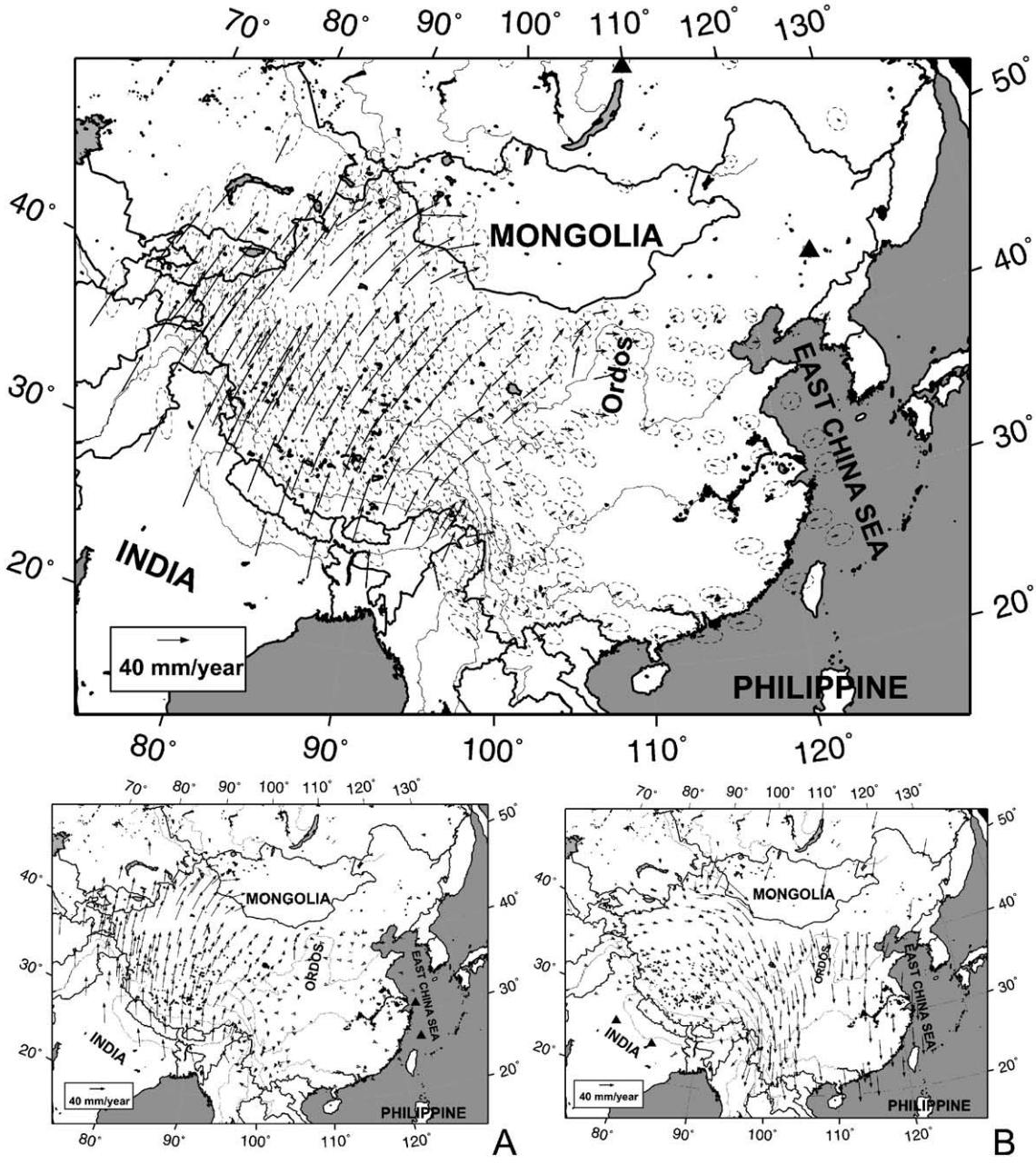

Fig. 5. The horizontal velocity field obtained for the studied area. The results are determined by fixing the two points shown by the solid triangles. The dashed ellipses give the one-sigma velocity errors. A and B present the corresponding motion patterns with southeastern China and India plate fixed, as respectively denoted by fixed points (solid triangles).

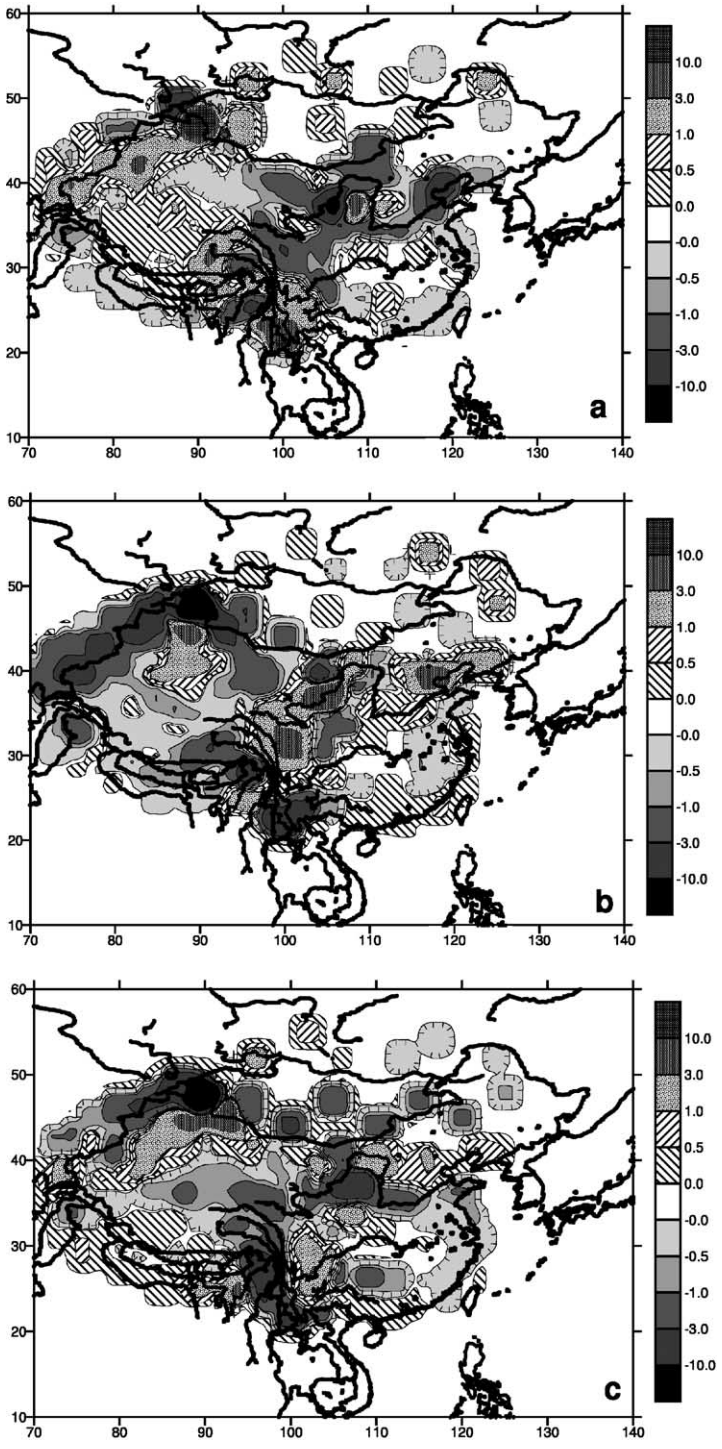

Fig. 6. Spatial distribution of the model strain rate calculated from relation (6), (a) ε_{xx}, (b) ε_{yy}, (c) ε_{xy}. The coordinate system of the notation corresponds to the local East(x)–North(y)–Up(z) system.

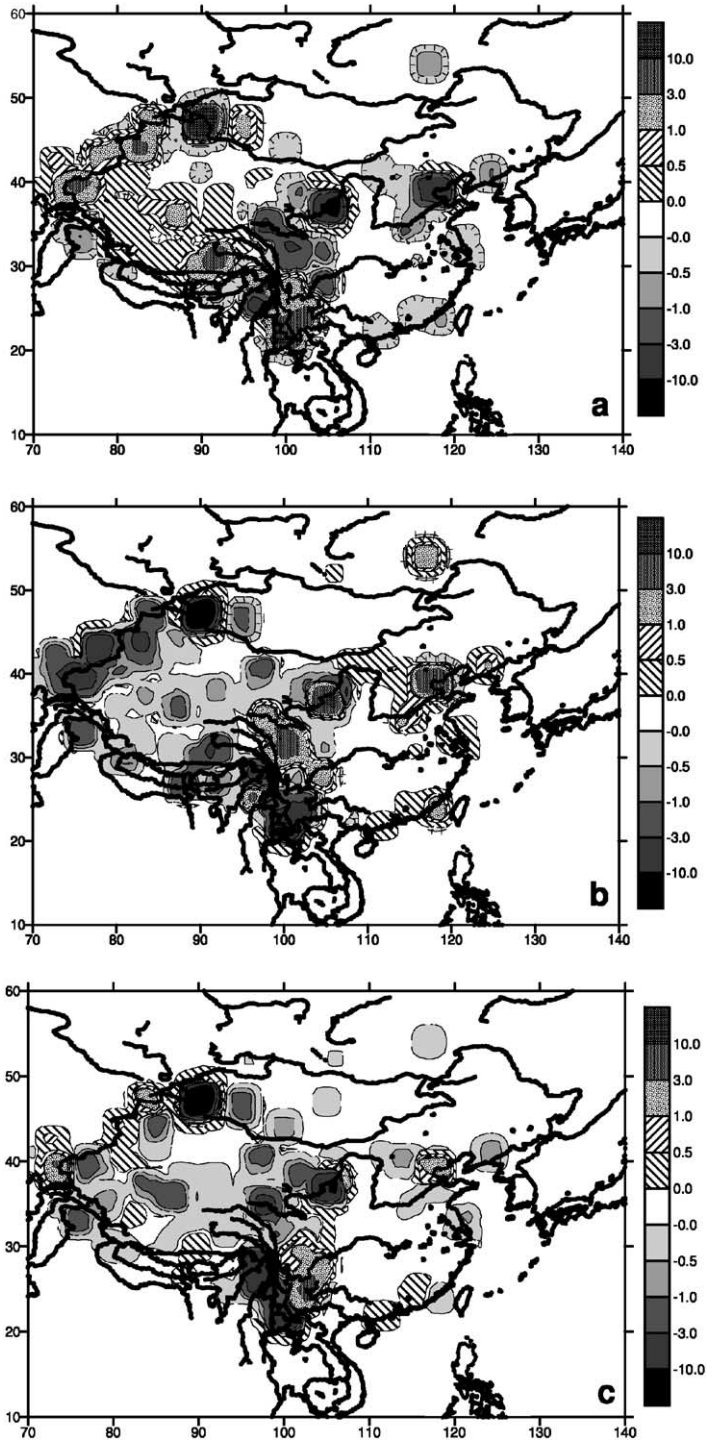

Fig. 7. Spatial distribution of the observed strain rate obtained from relation (2), (a) ε_{xx}, (b) ε_{yy}, (c) ε_{xy}.

Davenport, 1969), which allows the estimation of a and b values with quite high accuracy over a long time period. The b value, a relatively stable parameter in comparison with the a value (Qin et al., 1999a), is widely believed to be closely related to the tectonics (Mogi, 1967) and the stress field (Scholz, 1968; Wyss, 1973). Therefore, the b value was calculated for each of 10 different zones (Fig. 4), whereas the a value, a rapidly changing spatially parameter, which depends on the level of seismic activity (Rundle, 1989; Turcotte, 1989, 1992; Pacheco et al., 1992), was determined for each triangle. By substituting the maximum moment $M_{0,\max}$, and the a and b value into relation (4), the scalar moment rate can be obtained for each triangle.

3.2. Inversion of the velocity field

As previously mentioned, every polygonal seismic source was separated into several triangles so the finite element method could be applied, as this was described by England and Molnar (1997b). In order to obtain the velocities at the vertices of every triangle, linear deformation inside each triangle was assumed. If the horizontal velocities at three vertices are (u_i, v_i), (u_j, v_j) and (u_k, v_k) and the corresponding coordinates are (x_i, y_i), (x_j, y_j) and (x_k, y_k), then the velocity (u, v) at any point (x, y) inside the triangle can be estimated using the following interpolation functions (England and Molnar, 1997b):

$$u = N_i u_i + N_j u_j + N_k u_k$$

$$v = N_i v_i + N_j v_j + N_k v_k \tag{5}$$

where

$$N_l = \frac{1}{2\Delta}(a_l + b_l x + c_l y) \quad (l = i, j, k)$$

$$a_i = x_j y_k - x_k y_j$$

$$b_i = y_j - y_k$$

$$\times (i,\ j \text{ and } k \text{ change counterclockwise in circular permutation})$$

$$c_i = x_k - x_j$$

and Δ is the area of the triangle. The horizontal components of the strain rate at any point (x, y) inside

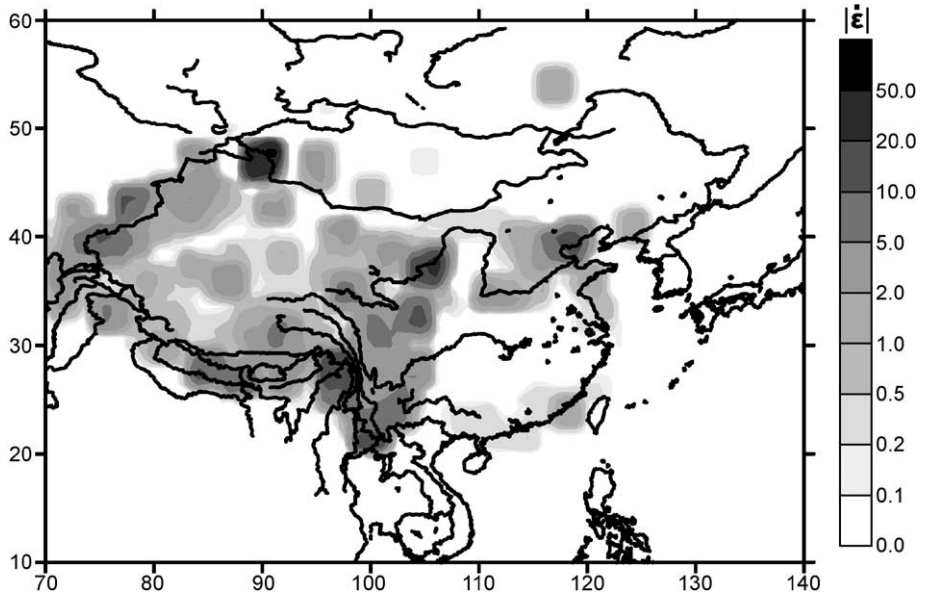

Fig. 8. Spatial distribution of the scalar strain rate $|\varepsilon|$ for the study area.

the triangle can also be obtained by the derivatives of Eq. (5):

$$\bar{\varepsilon}_{11} = \frac{\partial u}{\partial x} = \frac{1}{2\Delta}(b_i u_i + b_j u_j + b_k u_k)$$

$$\bar{\varepsilon}_{22} = \frac{\partial v}{\partial y} = \frac{1}{2\Delta}(c_i v_i + c_j v_j + c_k v_k)$$

$$\bar{\varepsilon}_{12} = \frac{1}{2}\left(\frac{\partial u}{\partial y} + \frac{\partial v}{\partial x}\right) = \frac{1}{4\Delta}(c_i u_i + b_i v_i + c_j u_j + b_j v_j + c_k u_k + b_k v_k) \quad (6)$$

For every triangle, three observations are available from the data, which represent the left-hand side of Eq. (6). In the case of m triangles and n nodes, the observation equation can be written in the matrix form:

$$AX = B \quad (7)$$

$$B = [b_j]^T = [\bar{\varepsilon}^1_{11}, \bar{\varepsilon}^1_{22}, \bar{\varepsilon}^1_{12}, \ldots, \bar{\varepsilon}^m_{12}]^T, X = [x_j]^T = [u_1, v_1, \ldots u_n, v_n]^T$$

$$A = [a_{ij}] = \begin{bmatrix} b_1 & 0 & b_2 & 0 & b_3 & 0 & : \\ 0 & c_1 & 0 & c_2 & 0 & c_3 & : \\ \frac{1}{2}c_1 & \frac{1}{2}b_1 & \frac{1}{2}c_2 & \frac{1}{2}b_2 & \frac{1}{2}c_3 & \frac{1}{2}b_3 & : \\ & & : & & & : & \\ & & : & & & : & \\ & & : & & & & : \end{bmatrix}_{3m\times 2n}$$

Eq. (7) is the final linear system to be solved for the determination of (u_i, v_i), which cannot be solved directly as matrix A has a zero determinant. This ill-conditioning reflects the fact that the velocity is a relative vector, which changes depending on the definition of a reference point. Hence, it is necessary to fix some points of the finite-element grid (triangle nodes) in order to define such a reference frame. England and Molnar (1997b) showed that at least two points must be chosen as fixed in order to solve this linear system (non-singular A). In order to study the possible existence of singularities or ill-conditioning of the matrix A, we have employed the Singular Value Decomposition (SVD) method (Lanczos, 1960; Press et al., 1992) for the solution of Eq. (7):

$$A = UWV^T \quad (8)$$

where U and V are orthogonal matrices and W contains the singular values of A. The horizontal velocities can be estimated by:

$$X = VW^{-1}U^T B \quad (9)$$

Table 2
Mean strain rates (eigenvalues), azimuths and direction-cosines of the three principal strain-rate axes for each of the 10 main seismotectonic zones shown in Fig. 4

	Eigenvalue	Azimuth	Direction-cosine		
Area A	0.1334e − 08	20.3	0.17	0.46	0.87
	− 0.1276e − 08	16.7	0.25	0.84	− 0.49
	− 0.5785e − 10	107.6	− 0.95	0.30	0.03
Area B	0.1199e − 09	79.5	0.98	0.18	0.00
	− 0.9589e − 10	− 9.2	0.02	− 0.15	− 0.99
	− 0.2405e − 10	169.5	− 0.18	0.97	− 0.15
Area C	0.2765e − 09	49.2	0.64	0.55	− 0.54
	− 0.2405e − 09	− 176.4	− 0.04	− 0.67	− 0.74
	− 0.3600e − 10	122.6	− 0.77	0.49	− 0.41
Area D	0.3891e − 10	− 0.1	0.00	− 1.00	0.10
	− 0.3269e − 10	− 104.5	− 0.36	− 0.09	− 0.93
	− 0.6210e − 11	92.1	− 0.93	0.03	0.36
Area E	0.5044e − 10	42.2	0.40	0.44	− 0.80
	− 0.5396e − 10	166.0	− 0.22	0.90	0.38
	0.3515e − 11	88.4	0.89	0.02	0.46
Area F	0.1188e − 09	− 177.2	− 0.01	− 0.24	0.97
	− 0.1149e − 09	38.4	0.61	0.77	0.20
	− 0.3913e − 11	− 53.2	0.79	− 0.59	− 0.14
Area G	0.2008e − 09	84.3	0.51	0.05	− 0.86
	− 0.2261e − 09	− 178.7	− 0.02	− 1.00	− 0.07
	0.2534e − 10	93.7	− 0.86	0.06	− 0.50
Area H	0.1239e − 08	159.6	− 0.06	0.15	0.99
	− 0.1478e − 08	178.5	− 0.03	0.99	− 0.15
	0.2386e − 09	− 92.0	− 1.00	− 0.03	− 0.05
Area I	0.3760e − 09	84.5	1.00	0.10	0.02
	− 0.5772e − 09	− 5.1	0.08	− 0.94	0.33
	0.2012e − 09	− 8.9	0.05	− 0.32	− 0.94
Area J	0.2347e − 09	− 5.3	0.09	− 0.99	0.13
	− 0.2139e − 09	− 97.6	− 0.95	− 0.13	− 0.28
	− 0.2084e − 10	108.8	− 0.30	0.10	0.95

In order to estimate the error ellipses of the velocity vectors (u, v) it is necessary to compute the covariance matrix of the solution, C_x. which can be obtained by:

$$C_x = VW^{-2}V^T\sigma_b^2 \tag{10}$$

where σ_b the fitting error, estimated by the misfit of Eq. (7) as $\sigma_b=[\Sigma(a_{ij}X_j - b_j)^2]^{1/2}$, which quantitatively describes how well the obtained velocity field describes the estimated (through Eq. (2)) strain-rate data.

It is well known that the local vorticity (rotation rate) cannot by directly obtained from the moment tensor summation, as ε_{ij} (derived from M_{ij}) contains only the symmetrical part of the velocity gradient tensor (e.g. Jackson and McKenzie, 1988). However, following the main idea of Haines (1982), we can indirectly obtain the vorticity from the interpolated velocity field, V, using the following equation:

$$\begin{aligned}\nabla \times V|_z &= \frac{1}{2}\left(\frac{\partial v}{\partial x} - \frac{\partial u}{\partial y}\right)\\ &= \frac{1}{4\Delta}(b_i v_i - c_i u_i + b_j v_j - c_j u_j\\ &\quad + b_k v_k - c_k u_k)\end{aligned} \tag{11}$$

where v and u are the velocities obtained from Eq. (7).

4. Calculation of velocity model

In order to proceed with the estimation of the velocity model, the reference frame has to be chosen. Since the northern part of the Eurasian plate is traditionally considered as "stable", exhibiting little seismicity (Jackson and McKenzie, 1984, 1988; Holt et

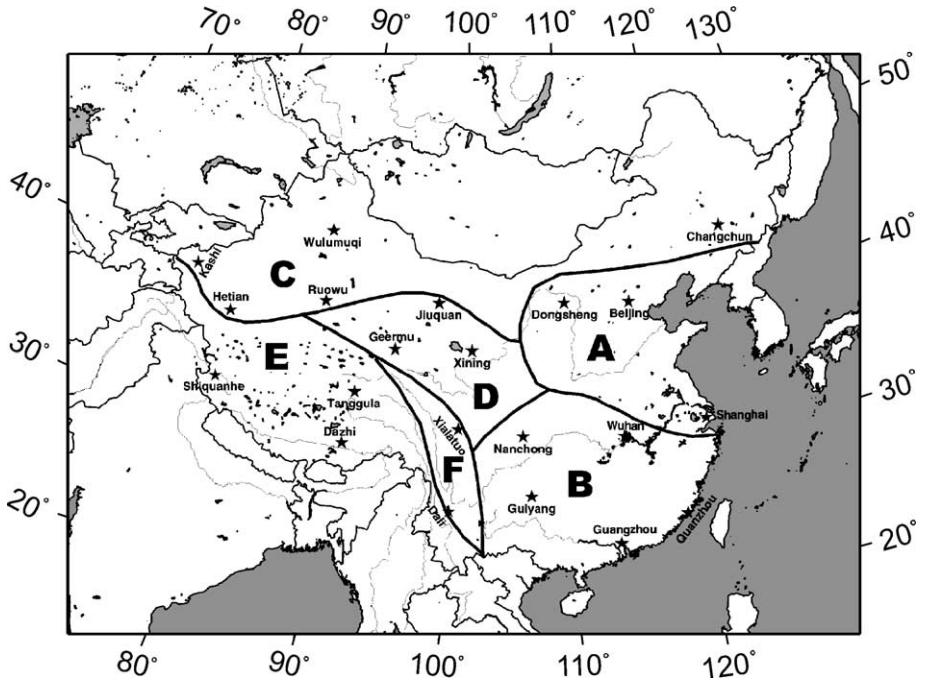

Fig. 9. The GPS sites' (denoted by asterisks) in the mainland of China and the six main GPS kinematic model zones outlined by the thick lines. Codes A, B, C, D, E, and F indicate the zones described in Table 3 (Zhang and Zhou, 1998; Zhou et al., 1998).

Table 3
Euler vectors of the kinematic model with respect to the Changchun station in northeast China (Zhang and Zhou, 1998; Zhou et al., 1998)

Region	Latitude	Longitude	× 0.001 (″) year^{-1}	ω_x	ω_y	ω_z
				(rad × 10^{-9} year^{-1})		
A	50°32′ 36″	107°40′ 59″	1.441	− 1.266	3.971	5.604
B	− 2°35′ 59″	− 63°55′ 49″	1.197	2.547	− 5.206	− 0.261
C	− 14°23′ 14″	− 80°37′ 57″	1.470	1.123	− 6.807	− 1.780
D	30°48′ 34″	60°54′ 51″	0.915	1.856	− 3.337	2.262
E	65°17′ 01″	44°35′ 24″	1.626	2.361	2.327	7.154
F	20°40′ 45″	− 80°39′ 11″	5.764	3.799	− 25.890	− 9.811

The coordinate system used corresponds to the East(x)–North(y)–Up(z) system.

al., 1995; Peltzer and Saucier, 1996; England and Molnar, 1997b; Zhang and Zhou, 1998) the fixed points were chosen to lie in this area, hence the velocity field computed here is considered as relative to stable Eurasia. We should point out that triangles/sources for which no seismicity data were available were considered as zero-strain areas, which have no contribution to the calculations except for acting only as a frame that connects nearby sources and "transfers" the velocity field across its borders, without changing it. The same approach was adopted for the few cases when no fault plane solutions were available, as these corresponded to very-low seismicity triangles/sources, which could also be considered as zero-strain areas.

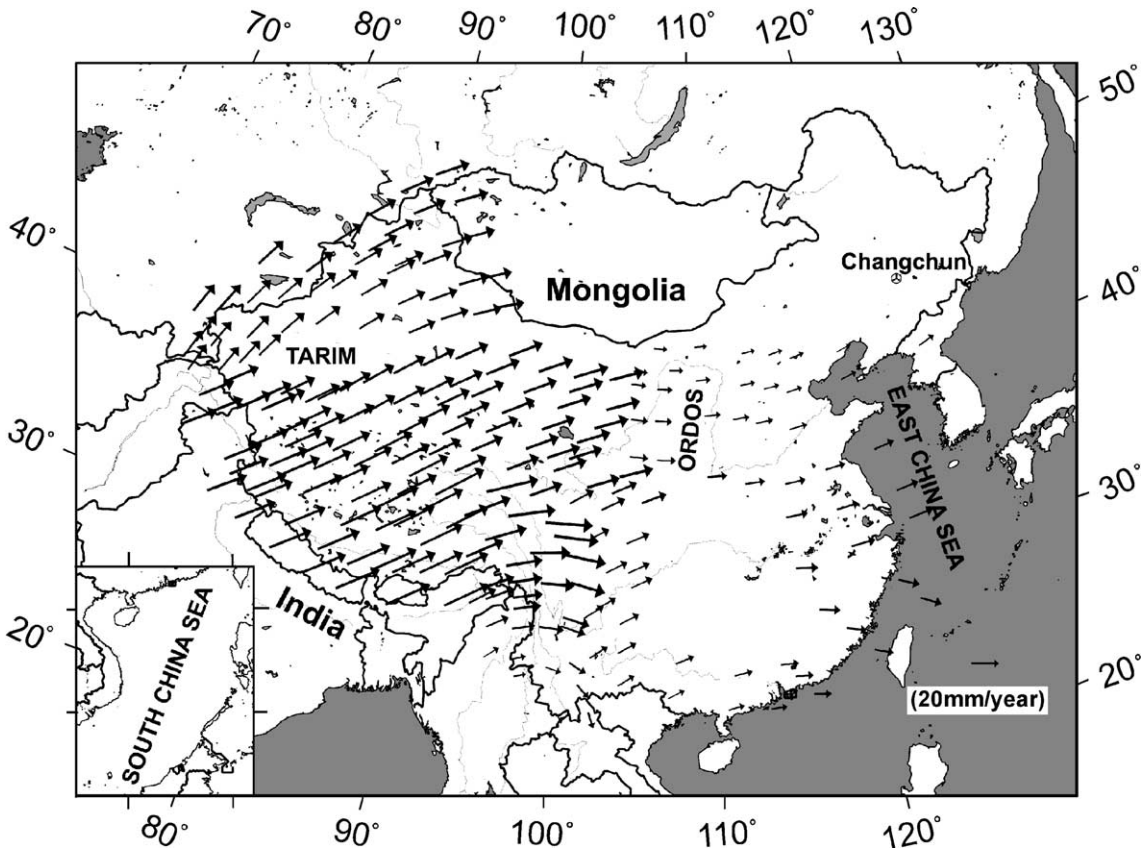

Fig. 10. The GPS velocity field, as it was obtained on the same nodes which are used for the seismic velocity field.

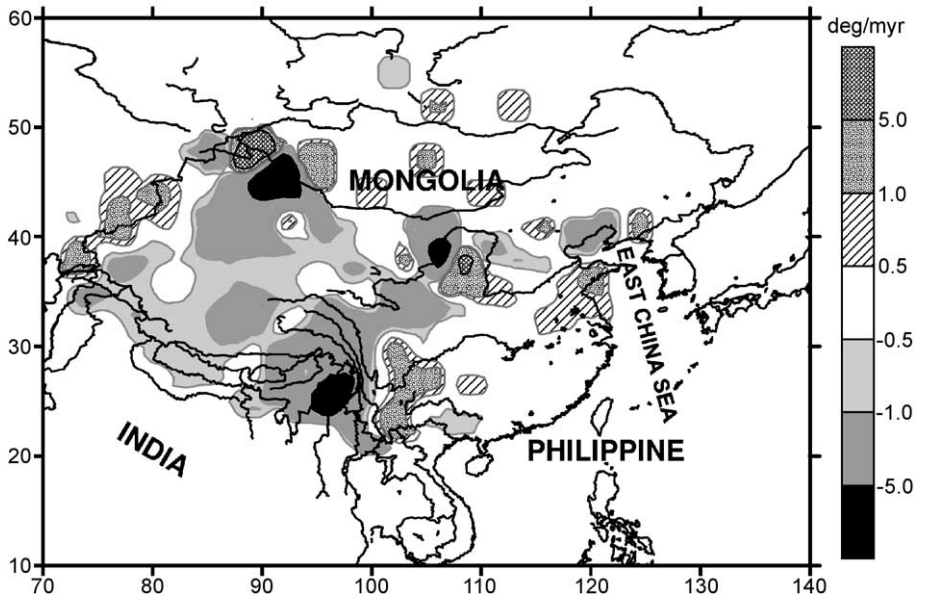

Fig. 11. Rotation rates calculated for the study area using relation (11). All value are reduced to degrees/million-year. Positive values correspond to counterclockwise rotations, whereas negative values to clockwise.

The finally obtained horizontal velocity field relative to the Eurasian plate is plotted in Fig. 5, where the two fixed reference points are also shown. The position of these fixed points on stable Eurasia was chosen to be in the vicinity of the Changchun GPS station, in order to facilitate the comparison of the obtained results with the GPS data later presented. In order to verify the efficiency and stability of the inversion, we have compared the model strain rate (Fig. 6), which was obtained from the right-hand side of relation (6) using the finally determined velocity, with the observed strain rate (left-hand side of Eq. (6)) determined from Eq. (2) (Fig. 7). In general, the comparison shows that the modeled strain rate is in very good agreement with the estimated strain rate data. It should be noted that in order to avoid numerical instabilities double precision accuracy was adopted in all calculations. The spatial distribution of the estimated scalar strain rate was calculated from the scalar seismic moment rate (Eq. (4)) and is also presented in Fig. 8. Furthermore, in order to exhibit the average characteristics of the stress field, the principal strain rates and their azimuths for the 10 main seismotectonic zones (Fig. 4) were also calculated and are given in Table 2.

In order to evaluate the reliability of the determined horizontal velocity field, we have compared the obtained results with existing GPS data. For this comparison, the most recent GPS kinematic model for the area of mainland of China was used, which was based on the observations made at 21 GPS stations throughout the main territory of China in the time period between 1994 and 1996 (Zhang and Zhou, 1998; Zhou et al., 1998). The location of the GPS observation sites as well as the regions of the GPS model are presented in Fig. 9, whereas the main model parameters are given in Table 3. On the basis of this GPS model, we have calculated the "expected" GPS velocities on every node of our zonation grid in the mainland of China and the final results are presented in Fig. 10. Finally, the rotational component of the velocity field was also estimated and is given in Fig. 11.

5. Discussion

The general motion pattern obtained with respect to the Eurasian plate complies with previous results (Holt et al., 1995; Westaway, 1995; Molnar and

Gipson, 1996; Peltzer and Saucier, 1996; Larson et al., 1999), with the most recent GPS model (Fig. 10) of Zhang and Zhou (1998) and Zhou et al. (1998) and with the results presented by field observations of the geologic survey of China (velocity arrows in China mainland shown in Fig. 1).

The results obtained with Eurasia fixed (Fig. 5) suggest that about the 50 mm/year of the convergence is expressed seismically as shortening across the Himalaya, which is in a very good agreement with the results of previous works (Molnar and Deng, 1984; Armijo et al., 1986; Molnar and Lyon-Caen, 1989). Global plate motion models (Demets et al., 1990, 1994), which predict that approximately 50 mm/year of northward directed convergence is taken up between India and Eurasia, in agreement with Westaway (1995) who suggests that the collision zone between India and Eurasian plate (~ 2500 km) has a convergence rate of 50 mm/year. It has been suggested that the thickening of the plateau and the eastward lateral-transport of material will accommodate India's penetration (Molnar and Gipson, 1996).

In southeastern boundary of Qiangzhang plateau, the velocity field rotates clockwise at a velocity of 25–30 mm/year, which is compatible with Westaway's (1995) estimate near the Xianshuihe region. The velocity "flow" follows the Xianshuihe fault, the Jinshajiang suture and the Red River and is then split into two branches: one maintains a clockwise rotating pattern in the southeast part of Tibet to compensate the Indian penetration (Holt et al., 1991) and the other has an counterclockwise rotation in the southeastern part of China. Westaway (1995) suggests that flow of lower crust from India to Tibet is causing its crustal thickening, and flow from Tibet to Yunnan is carrying the upper crust eastward, causing the extension of Tibet and the associated strike–slip faulting. This pattern is in a very good agreement with the results obtained in the present study. Finally, in the region of western border of China, the velocity is more or less constant, with India's convergence ranging from about 30 up to 50 mm/year.

If we divide the western China (longitude < 110°) into three main parts, namely the western (Long. < 80°), middle (80° < Long. < 100°) and eastern (Long.>100°) part, we can see that the western part moves dominantly northward from Kashi towards the western Tien Shan region. In the middle part, the motion gradually shows a smaller northward component while the eastward component increases from south to north. The motion pattern near the northern boundary of China shows the clockwise rotation component (Fig. 5). The eastern part, however, has the most complicated motion pattern. The sudden reduction of the eastward motion to its eastern margin supports the treatments of the continental lithosphere as a thin viscous sheet whose strength is governed primarily by power law creep in the upper mantle (Molnar and Gipson, 1996; England and Molnar, 1997a). The Longmenshan thrust fault (Fig. 1) in eastern boundary of the Tibet plateau plays a complicated role in the motion pattern, as it hampers the eastward motion and forces the lithosphere to move in both directions parallel to the fault (Fig. 5). The velocity reduces to about 8 mm/year in Shanghai, east of China, which is in a reasonable agreement with VLBI results (Molnar and Gipson, 1996) and GPS results (Zhang and Zhou, 1998; Zhou et al., 1998; Larson et al., 1999). Generally, the present result is compatible with Zhang and Zhou's (1998) results (Fig. 10). The GPS motion pattern (Zhang and Zhou, 1998; Zhou et al., 1998) near the Xianshuihe and the Red River region is quite similar with the results obtained in the present study, although important differences exist in the detailed motion pattern between the two studies. The GPS results seem to overestimate the velocity in the eastern part of China (e.g. Shanghai ~ 18 mm/year) and underestimate the convergence of the India plate (about 36 mm/year), probably due to the sparse station coverage and the short observation time (2 or 3 years).

Comparing the motion pattern (Fig. 5) with the scalar strain rate (Fig. 8), it is evident that the large gradient of the velocity (i.e. the sudden change of the motion direction) are in a good agreement with sharp changes of the strain rate, i.e. the strong earthquakes, as expected since strain is the velocity gradient. For example, the 1950 Assam earthquake ($M = 8.6$) in the eastern Himalaya Syntaxis, the 1931 Fuyun earthquake ($M = 7.7$) around northern Tien Shan, and several strong events along the Qilianshan fault (1920 Haiyuan earthquake, $M = 8.4$; 1927 Gulang earthquake, $M = 7.7$; 1932 Changma earthquake $M = 7.5$) dominate the strain rate released in their region.

The rotation results show that most of the western part of China is dominated by clockwise rotation (Figs.

5 and 11). Recent GPS results for the Xianshuihe region also showed that it's clockwise at about 10 mm/year (Chen et al., 2000), whereas Xu and Deng (1996), using geological data, suggest that the Xianshuihe and Kunlun faults have a clockwise rotation rate of 9–12°/ma during the Holocene, which is compatible with the present result. The southeastern part of Ordos block is rotating counterclockwise at <5°/ma, which is in a good agreement with the paleomagnetic results of 1.3–6.3° (Xu et al., 1994). The region along the western border of China, however, is mostly controlled by the counterclockwise rotation (Fig. 11), which was also confirmed by England and Molnar (1997b). The rotation pattern near the southeast Tibet plateau along the Red River is rather complicated, where its western part shows a clockwise pattern, which forms a "vortex" and its eastern part moves counterclockwise. The combination of these motion patterns allows the partial accommodation of the material "pushed-in" by the India plate.

Acknowledgements

We would like to express our sincere appreciation to B.C. Papazachos for his useful suggestions and kind help and to G.F. Karakaisis for checking the draft. We would also like to thank R. Westaway and R. Fu for their comments and suggestions, which significantly helped to improve the quality of the paper. Our gratitude is also extended to Jin Xuesheng of Seismological Bureau of Hebei Province, SSB, China for providing some of the data. This work is partially supported by the project of the Gen. Sectr. Res. and Techn. of Greece under the contract EPAN-M.4.3_2013555. Some of the figures were made using the GMT software (Wessel and Smith, 1995).

References

Abe, K., 1981. Magnitudes of large earthquakes from 1904 to 1980. Phys. Earth Planet. Inter. 27, 72–93.

Aki, K., Richards, P.G., 1980. Quantitative Seismology Theory and Methods. Freeman, New York.

Ambraseys, N.N., Jackson, J.A., 1997. Seismicity and strain in the gulf of Corinth (Greece) since 1694. J. Earth Eng. 1, 433–474.

Armijo, R., Tapponnier, P., Mercier, J.L., Tonglin, H., 1986. Quaternary extension in southern Tibet. J. Geophys. Res. 91, 13803–13872.

Avouac, J.P., Tapponier, P., Bai, M., You, H., Wang, G., 1993. Active thrusting and folding along the northern Tien Shan and late cenozoic rotation of Tarim relative to Dzungaria and Kazakhstan. J. Geophys. Res. 98, 6755–6804.

Chen, W.-P., Molnar, P., 1977. Seismic moments of major earthquakes and the average rate of slip in central Asia. J. Geophys. Res. 82, 2945–2969.

Chen, Z., Burchfiel, B.C., Liu, Y., King, R.W., Royden, L.H., Tang, W., Wang, E., Zhao, J., Zhang, X., 2000. Global Positioning System measurements from eastern Tibet and their implications for India/Eurasia intercontinental deformation. J. Geophys. Res. 105, 16215–16227.

Demets, C., Gordon, R.G., Argus, D.F., Stein, S., 1990. Current plate motions. Geophys. J. Int. 101, 425–478.

Demets, C., Gordon, R.G., Argus, D.F., Stein, S., 1994. Effect of recent revisions to the geomagnetic reversal time scale on estimates of current plate motions. Geophys. Res. Lett. 21, 2191–2194.

Deng, Q., Xu, X., Yu, G., 1994. Characteristics of regionalization of active faults in China and their genesis. Act. Fault Res. China 1–14 (in Chinese).

Ekstrom, G., Dziewonski, A., 1988. A very broad band analysis of the Michoacan, Mexico, earthquake of September 19, 1985. Geophys. Res. Lett. 13, 605–608.

England, P., Houseman, G., 1988. The mechanics of the Tibetan plateau. Philos. Trans. R. Soc. London, Ser. A 326, 301–320.

England, P., Molnar, P., 1997a. Active deformation of Asia: from kinematics to dynamics. Science 278, 647–650.

England, P., Molnar, P., 1997b. The field of crustal velocity in Asia calculated from Quaternary rates of slip on faults. Geophys. J. Int. 130, 551–582.

Gao, M., 1996. A study on recent geodynamics at the southeastern margin of the Qinghai–Xizhang (Tibet) plateau. Seismol. Geol. 18, 129–142 (in Chinese).

Haines, A.J., 1982. Calculating velocity fields across plate boundaries from observed shear rates. Geophys. J. R. Astron. Soc. 68, 203–209.

Haines, A.J., Holt, W.E., 1993. A procedure for obtaining the complete horizontal motions within zones of distributed deformation from the inversion of strain rate data. J. Geophys. Res. 98, 12057–12082.

Holt, W.E., Ni, J.F., Wallace, T.C., Haines, A.J., 1991. The active tectonics of the Eastern Himalayan Syntaxis and surrounding regions. J. Geophys. Res. 96, 14595–14632.

Holt, W.E., Li, M., Haines, A.J., 1995. Earthquake strain rates and instantaneous relative motions within central and eastern Asia. Geophys. J. Int. 122, 569–593.

Houseman, G., England, P., 1993. Crustal thicking versus lateral expulsion in the Indian–Asian continent collision. J. Geophys. Res. 98, 12233–12249.

Jackson, J., McKenzie, D., 1984. Active tectonics of the Alpine Himalayan Belt between western Turkey and Pakistan. Geophys. J. R. Astron. Soc. 77, 185–264.

Jackson, J., McKenzie, D., 1988. The relationship between plate motions and seismic moment tensors, and the rates of active deformation in the Mediterranean and Middle East. Geophys. J. 93, 45–73.

Kanamori, H., 1977. The energy release in great earthquakes. J. Geophys. Res. 82, 2981–2987.

Kearey, P., Vine, F.J., 1990. Global Tectonics. Blackwell, Oxford.

Kostrov, V.V., 1974. Seismic moment and energy of earthquakes and seismic flow of rock. Izv. Acad. Sci. USSR Phys. Solid Earth 1, 23–44.

Lanczos, C., 1960. Linear Differential Operators. Van Nostrand, New York, p. 546.

Larson, K.M., Burgmann, R., Bilham, R., Freymueller, J.T., 1999. Kinematics of the India–Eurasia collision zone from GPS measurements. J. Geophys. Res. 104, 1077–1093.

Ma, X., 1987. An Introduction to the Lithospheric Dynamics in China, Introduction of Dynamic Map of China. Geological Press, Beijing, in Chinese.

Madariaga, R., 1983. Earthquake source theory: a review. Proceedings of the International School of Physics, Course LXXXV, pp. 1–44.

Milne, W.G., Davenport, A.G., 1969. Determination of earthquakes risk in Canada. Bull. Seismol. Soc. Am. 59, 729–754.

Mogi, K., 1967. Regional variations in magnitude–frequency relation of earthquake. Bull. Earthquake Res. Inst. 45, 313–325.

Molnar, P., 1979. Earthquake recurrence intervals and plate tectonics. Bull. Seismol. Soc. Am. 69, 115–133.

Molnar, P., 1983. Average regional strain due to slip on numerous faults of different orientations. J. Geophys. Res. 88, 6430–6432.

Molnar, P., Deng, Q., 1984. Faulting associated with large earthquakes and the average rate of deformation in Central and Eastern Asia. J. Geophys. Res. 89, 6203–6227.

Molnar, P., Gipson, J.M., 1996. A bound on the rheology of continental lithosphere using very long baseline interferometry: the velocity of south China with respect to Eurasia. J. Geophys. Res. 101, 545–553.

Molnar, P., Lyon-Caen, H., 1989. Fault plane solutions of earthquakes and active tectonics of the Tibetan plateau and its margins. Geophys. J. Int. 99, 123–153.

Pacheco, J.F., Sykes, L.R., 1992. Seismic moment catalog of large shallow earthquakes, 1900 to 1989. Bull. Seismol. Soc. Am. 82, 1306–1349.

Pacheco, J.F., Scholz, C.H., Sykes, L.R., 1992. Changes in frequency–size relationship from small to large earthquakes. Nature 355, 71–73.

Papazachos, C.B., Kiratzi, A.A., 1992. A formulation for reliable estimation of active crustal deformation and its application to central Greece. Geophys. J. Int. 111, 424–432.

Peltzer, G., 1988. Centrifuged experiments of continental scale tectonics in Asia. Geological Kinematics and Dynamics. Bull. Geol. Inst. Univ. Uppsala, vol. 14, pp. 115–128.

Peltzer, G., Saucier, F., 1996. Present-day kinematics of Asia derived from geologic fault rates. J. Geophy. Res. 101, 27943–27956.

Press, W.H., Teukolsky, S.A., Vetterling, W.T., Flannery, B.P., 1992. Numerical Recipes in Fortran: The Art of Scientific Computing. Cambridge Univ. Press, New York, 963 pp.

Qin, C.Y., Papadimitriou, E.E., Papazachos, B.C., Karakaisis, G.F., 1999a. Spatial distribution of time independent seismicity of China. Pure Appl. Geophys. 154, 101–119.

Qin, C.Y., Papadimitriou, E.E., Papazachos, B.C., Karakaisis, G.F., 1999b. On the validity of the regional time and magnitude predictable model in China. Ann. Geofis. 42 (5).

Qin, C.Y., Papadimitriou, E.E., Papazachos, B.C., Karakaisis, G.F., 2001. Time-dependent seismicity and long-term prediction in China. J. Asian Earth Sci. 19, 97–128.

Research Group of SSB, 1988. Active Fault System Around Ordos Massif Seismological Press, Beijing, China, in Chinese.

Rundle, J.B., 1989. Derivation of the complete Gutenberg–Richter magnitude–frequency relation using the principle of scale invariance. J. Geophys. Res. 94, 12337–12342.

Savage, J.C., Simpson, R.W., 1997. Surface strain accumulation and the seismic moment tensor. Bull. Seismol. Soc. Am. 87, 1345–1353.

Scholz, C.H., 1968. The frequency magnitude relation of microfracturing in rock and its relation to earthquakes. Bull. Seismol. Soc. Am. 58, 399–415.

Turcotte, D.L., 1989. A fractal approach to probabilistic seismic hazard assessment. Tectonophysics 167, 171–177.

Turcotte, D.L., 1992. Fractals and Chaos in Geology and Geophysics. Cambridge Univ. Press, New York, pp. 35–50.

Ward, S.N., 1998a. On the consistency of earthquake moment rates, geological fault data, and space geodetic strain: the United States. Geophys. J. Int. 134, 172–186.

Ward, S.N., 1998b. On the consistency of earthquake moment rates and space geodetic strain rates: Europe. Geophys. J. Int. 135, 1011–1018.

Wen, L.X., Anderson, D.L., 1997. Present-day plate motion constraint on mantle rheology and convection. J. Geophys. Res. 102, 24639–24653.

Wessel, P., Smith, W.H.F., 1995. The Generic Mapping Tools (GMT) software.

Westaway, R., 1991. Discussion of and correction to: deformation of the NE basin and Range Province: the response of the lithosphere to the Yellowston plume. Geophys. J. Int. 104, 647–659.

Westaway, R., 1995. Crustal volume balance during the India–Eurasia collision and altitude of the Tibetan plateau: a working hypothesis. J. Geophys. Res. 100, 15173–15194.

Wyss, M., 1973. Towards a physical understanding of the earthquake frequency distribution. Geophys. J. R. Astron. Soc. 31, 341–359.

Xu, X., Deng, Q., 1996. Nonlinear characteristics of paleoseismicity in China. J. Geophys. Res. 101, 6209–6231.

Xu, X., Chen, G., Xu, M., Sun, Y., Han, Z., 1994. Rotation model and dynamics of blocks in the North China and its adjacent areas. Earth Sci. J. China Univ. Geosci. 19, 129–138 (in Chinese with English abstract).

Zhang, Y.G., Zhou, S.Y., 1998. Study on current kinematic model of intraplate rigid blocks. Crustal Deform. Earthquake 18, 8–13 (in Chinese).

Zhou, S.Y., Zhang, Y.G., Ding, G.Y., Wu, Y., Qin, X.J., Shi, S.Y., Wang, Q., Yiu, X.Z., Qiao, X.J., Shuai, P., Deng, G.J., 1998. The plate motion model of Chinese mainland based on the GPS data. Acta Seismol. Sin. 20, 347–355 (in Chinese).